

# PointNorm: Normalization is All You Need for Point Cloud Analysis

Shen Zheng  
Carnegie Mellon University  
Pittsburgh, PA, USA  
shenzhen@andrew.cmu.edu

Jinqian Pan  
New York University  
New York, NY, USA  
jp6218@nyu.edu

Changjie Lu  
Wenzhou-Kean University  
Wenzhou, Zhejiang, China  
lucha@kean.edu

Gaurav Gupta  
Wenzhou-Kean University  
Wenzhou, Zhejiang, China  
ggupta@kean.edu

## Abstract

Point cloud analysis is challenging due to the irregularity of the point cloud data structure. Existing works typically employ the ad-hoc sampling-grouping operation of PointNet++, followed by sophisticated local and/or global feature extractors for leveraging the 3D geometry of the point cloud. Unfortunately, those intricate hand-crafted model designs have led to poor inference latency and performance saturation in the last few years. In this paper, we point out that the classical sampling-grouping operations on the irregular point cloud cause learning difficulty for the subsequent MLP layers. To reduce the irregularity of the point cloud, we introduce a DualNorm module after the sampling-grouping operation. The DualNorm module consists of Point Normalization, which normalizes the grouped points to the sampled points, and Reverse Point Normalization, which normalizes the sampled points to the grouped points. The proposed PointNorm utilizes local mean and global standard deviation to benefit from both local and global features while maintaining a faithful inference speed. Experiments on point cloud classification show that we achieved state-of-the-art accuracy on ModelNet40 and ScanObjectNN datasets. We also generalize our model to point cloud part segmentation and demonstrate competitive performance on the ShapeNetPart dataset. Code is available at <https://github.com/ShenZheng2000/PointNorm-for-Point-Cloud-Analysis>.

## 1. Introduction

A point cloud is a group of points for describing the object shapes in the 3D space. Due to its importance for many downstream applications, such as autonomous driving [4], virtual and augmented reality [26], and robotics [30], point

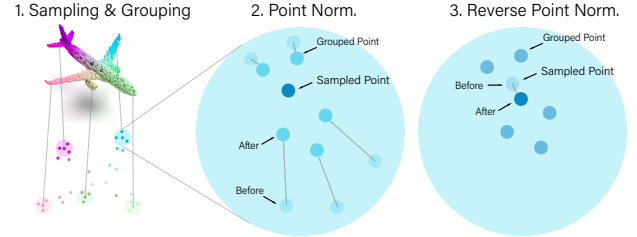


Figure 1. Overview of Point Normalization and Reverse Point Normalization in our PointNorm framework. After sampling and grouping, we first normalize the grouped points to the sampled points and then normalize the sampled points to the grouped point. In this way, we address the irregularity of the raw point cloud and thus make learning easier for the subsequent layers.

cloud analysis has recently gain enormous popularity in the computer vision community. However, point clouds are irregular (i.e., unevenly distributed), which makes learning their 3D geometry challenging [32].

The pioneering work PointNet [31] attempts to process each point in the point cloud independently with multi-layer perceptions (MLPs). The follow-up approach PointNet++ [32] further introduce set abstraction layers to exploit the local geometry. Specifically, the set abstraction layers consist of a sampling layer, a grouping layer, and a PointNet layer for non-linear mapping. The sampling layer (e.g., Farthest Point Sampling [25]) is used to select the representative points, whereas the grouping layer (e.g., K-Nearest Neighbors [29]) is employed to select the points closest to the representative points.

Inspired by PointNet++, a handful of works have attempted to exploit the local geometry of point cloud by incorporating convolution [44, 47], graph [43, 19], transformers [6, 56] or geometric methods [23, 34] in the non-linear

mapping layers. Meanwhile, many researchers have exploited the global geometry of the point cloud, using adaptive sampling [51], mesh [14], curve [46], or surfaces [34]. Unlike the local geometry, the global point features bring long-range semantics, which is particularly useful for part segmentation and semantic segmentation tasks [51, 46, 3].

Despite their progresses, both local and global approaches use sophisticated feature extractors and complicated optimization processes, which results in poor inference latency. This is unacceptable for large-scale point cloud analysis [15] and mobile point cloud analysis [30], which both value computational efficiency.

Besides, both approaches readily follow the ad-hoc sampling-grouping operations proposed by PointNet++ without carefully considering the irregularity of the point cloud data structure. The sampling-grouping operation’s failure to well capture the 3D geometry of the irregular point cloud leads to learning difficulty for the subsequent non-linear mapping layers. The performance saturation therefore occurs since however delicate the design is for the non-linear mapping layers, the inevitably performance drop from the sampling-grouping operations will prevent the model from reaching better results.

In this paper, we seek to get rid of complicated local and/or global feature extractors and develop a simple, intuitive network for point cloud analysis. Inspired by how normalization serves as a pre-processing step to address irregular data in 2D image processing [28, 11], we propose to add normalization operations after<sup>1</sup> the sampling-grouping operation, but *before* the non-linear mapping layers. In this way, we can enjoy the efficiency of the sampling-grouping operation while preventing the irregular data passing into the subsequent non-linear mapping layers. Since sampled and grouped points are both crucial for point cloud feature learning, it is hard to decide which one to normalize. Instead of discarding any one of them, we attempt to utilize both points using a novel module called DualNorm. As shown in Fig. 1, the DualNorm module first normalizes the grouped points to the sampled points and then normalizes the sampled points to the grouped points. Using local mean and global standard deviation in the normalization allows the proposed method to leverage both local and global features while still enjoying a faithful inference speed. Finally, we designed a novel Controllable Residual [9] Block (C-Resblock). Inspired by squeeze-excitation network [10] and inverted residual block [35], C-Resblock has a bottleneck ratio that can either squeeze or expand the model without significantly affecting the model performance. This allows us to develop lightweight versions with an elegant trade-off between model performance and model size. The contribu-

<sup>1</sup>We do not consider normalization before the sampling-grouping operation as it is extremely time consuming to process all point cloud at the beginning.

tions of this paper can be summarized as below:

- We propose a new framework named PointNorm. With local mean and global standard deviation, PointNorm eliminates the need for sophisticated local and global feature extractors, thereby significantly enhancing the computational efficiency.
- We introduce a novel module called DualNorm. By normalizing sampled points and grouped points to each other, we address the irregularity of point cloud and make learning point cloud features easier for the subsequent MLP layers.
- We design a plug-and-play style Controllable Residual Block (C-Resblock) to effectively trade-off between model performance and model size.
- We demonstrate our method achieves state-of-the-art performances on point cloud classification and segmentation tasks.

## 2. Related Work

### 2.1. Point Cloud Analysis

Due to the irregularity of the point cloud data structure, prior works attempt to transform the raw point cloud into intermediate voxels [24, 57], or multi-view images [55, 8], thereby converting the 3D challenge to a well-investigated 2D task. However, these transformations are accompanied by heavy computation and loss of shape details [52, 3]. PointNet [31] is the pioneering method that operates directly upon the raw point cloud. Based upon PointNet, PointNet++ [32] add a sampling-grouping operation before the MLP layers to extract the local geometry. Like PointNet++, and the follow-up works [17, 20, 44, 23], our PointNorm utilizes the sampling-grouping operation with a MLP-based architecture. The major difference between PointNorm and others is that PointNorm has normalization operations between the sampling-grouping layers and the MLP layers to cope with the irregular point cloud effectively and efficiently.

### 2.2. Point Cloud Local Geometry Exploration

Owing to the success of PointNet++, recent research has paid significant attention to local geometry exploration. The local geometry exploration methods can be grouped into four major categories: convolution-based [44, 47], graph-based [43, 19], transformer-based [6, 19], and geometry-based [23, 34]. The most prominent convolution-based method is PointConv [44], which utilizes MLPs and density functions to obtain the weight function for a given point. Unlike convolution-based methods, graph-based methods like EdgeConv [43] treat each point as a graph node and

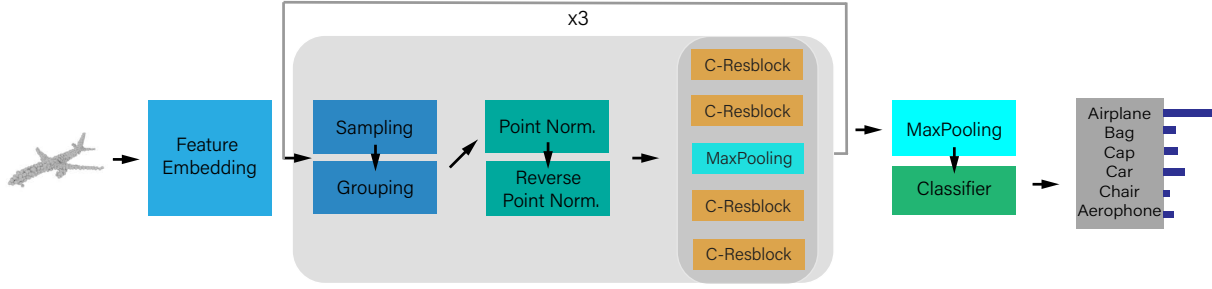


Figure 2. The workflow of PointNorm for classification tasks. Given an input point cloud, PointNorm first embeds the points features and then uses the sampling-grouping operation and the DualNorm module to obtain and normalize the sampled and grouped points. A list of Controllable Residual Blocks will then exploit the hierarchical features, which helps the classifier to model the correct category.

utilize graph edges to capture the local geometry between a specific point and its neighbors, whereas the transformer-based methods [6, 56] like Point Transformer [56] utilize self-attention in the transformer backbones to extract the local neighborhoods around each point. Different from other categories, the geometry-based is more customized. For example, PointMLP [23] utilizes a geometric affine module to adaptively translate the points in a local region, whereas Repsurf [34] leverages representative surfaces to describe the points in a local region explicitly. Unlike these methods requiring sophisticated local feature extractors, PointNorm only needs normalization operations using local neighbor points for calculating the mean.

### 2.3. Point Cloud Global Geometry Extraction

The attempt to extract global geometry in point cloud is predominantly inspired by the success of non-local network [42] in 2D image processing. The main challenge of point cloud global geometry extraction is how to effectively aggregate the local and the global features [46, 7]. To this end, PointASNL [51] introduces a local-nonlocal module with adaptive sampling to capture both the local and global dependencies of the sampled point. MeshWalker [14] utilizes random walks along the mesh surfaces to explore the local and global geometry. In contrast, CurveNet [46] develops a curve-based guided walk strategy to group and aggregate local and non-local point features. The aforementioned methods require sophisticated searching and optimization to extract and aggregate the local and global features, leading to poor inference latency. In comparison, the proposed PointNorm is quite efficient because it only needs normalization operations using global points (i.e., all points) for calculating the standard deviation.

## 3. Proposed Methods

In this section, we first introduce the DualNorm module and then employ standard deviation analysis to show how DualNorm addresses irregular point clouds. After that, we illustrate the model architecture for PointNorm. Finally, we introduce our Controllable Residual Block and show how it helps us to build a powerful lightweight version named PointNorm-Tiny.

### 3.1. DualNorm

PointNet++ [32] performs both sampling and grouping operations on the irregular point cloud. Consequently, the sampled and grouped points are both irregular. Our DualNorm modules consists of Point Normalization (PN) and Reverse Point Normalization (RPN). Specifically, PN aims to address the irregularity of the grouped points, whereas RPN aims to address the irregularity of the sampled points. Suppose  $x_s$  is the sampled points;  $x_g$  is the grouped points;  $k$  is the number of neighbors in the KNN algorithm [29];  $n$  is the number of points in a point cloud;  $d$  is the dimension (i.e., the channel number at a specific layer);  $\alpha_1$  and  $\alpha_2$  are learnable parameters initialized with a value of 1;  $\beta_1$  and  $\beta_2$  are learnable parameters initialized with a value of 0; and  $\varepsilon$  is set as  $1e-5$  to promote numerical stability (e.g., avoid division by zero). In the following two paragraphs, we derive the formulation for PN and PRN, considering both the local and the global choices.

**Point Normalization (PN)** normalizes the grouped points  $x_g$  to the sampled points  $x_s$ . The local mean is  $\mu_s = x_s$ , and the global mean is  $\mu_s = \frac{1}{nd} \sum_{b=1}^n \sum_{c=1}^d x_{g_{a,b,c}}$ . Meanwhile, the local standard deviation is  $\sigma_1 = \sqrt{\frac{1}{k} \sum_{a=1}^k [x_{g_a} - \mu_s]^2}$ , and the global standard deviation is  $\sigma_1 = \sqrt{\frac{1}{knd} \sum_{a=1}^k \sum_{b=1}^n \sum_{c=1}^d [x_{g_{a,b,c}} - \mu_s]^2}$ . The scale-and-shift strategy in batch normalization [12] is em-

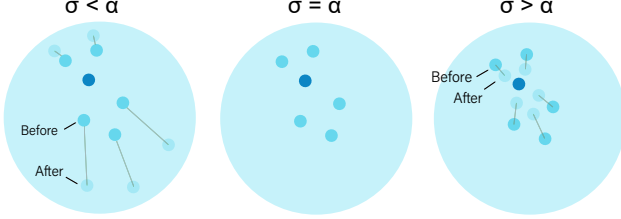


Figure 3. Illustration of how PointNorm customize the strategy for irregular point cloud according to the numerical relationship between local/global standard deviation  $\sigma$  and the learnable parameter  $\alpha$ .

ployed to promote non-linearity and to make the PN layers trainable in the backpropagation process. The scale-and-shift normalization for PN is  $x_g \leftarrow \alpha_1 * \frac{x_g - \mu_s}{\sigma_1 + \varepsilon} + \beta_1$ .

**Reverse Point Normalization (RPN)** normalizes the sampled points  $x_s$  to the grouped points  $x_g$ . The local mean is  $\mu_g = \frac{1}{k} \sum_{a=1}^k x_g$ , and the global mean is  $\mu_g = \frac{1}{knd} \sum_{a=1}^k \sum_{b=1}^n \sum_{c=1}^d x_g$ . The local standard deviation is not straightforward to calculate in RPN because we only have one sampled point for a KNN-group, and there is no way to calculate the standard deviation with a single point. Instead, we consider the absolute value of the L1 distance between  $\mu_g$  and  $x_s$ , and use a square root function to promote non-linearity. The local standard deviation is therefore formulated as  $\sigma_2 = \sqrt{|x_s - \mu_g| + \varepsilon}$ . Since there is always more than one sampled point in a batch, the global standard deviation can be formulated naturally like we did for PN. The global standard deviation is  $\sigma_2 = \sqrt{\frac{1}{knd} \sum_{a=1}^k \sum_{b=1}^n \sum_{c=1}^d [x_{s,a,b,c} - \mu_g]^2}$ , and the scale-and-shift normalization for RPN is  $x_s \leftarrow \alpha_1 * \frac{x_s - \mu_g}{\sigma_2 + \varepsilon} + \beta_2$ .

**Standard Deviation Analysis** We analyze the standard deviation change of point cloud during DualNorm to understand how DualNorm address the irregularity of point cloud. Let's take PN as a example, since RPN can be done in a similar way due to the symmetry of PN and RPN. Suppose that the grouped points before and after PN is  $x_g$  and  $x_{\hat{g}}$ , and the standard deviation for  $x_g$  and  $x_{\hat{g}}$  is  $\sigma_{x_g}$  and  $\sigma_{x_{\hat{g}}}$ . According to the scale-and-shift normalization, we have:

$$x_{\hat{g}} = \alpha_1 * \frac{x_g - \mu_s}{\sigma_1 + \varepsilon} + \beta_1 \quad (1)$$

If we ignore the tiny  $\varepsilon$ , we can express  $\sigma_{x_{\hat{g}}}$  as:

$$\sigma_{x_{\hat{g}}} = \frac{\alpha}{\sigma_1} * \sigma_{x_g} \quad (2)$$

Suppose that the standard deviation change ratio is defined as  $\Delta = \frac{\sigma_{x_{\hat{g}}}}{\sigma_{x_g}}$ . Equ. 2 can therefore be written as:

$$\Delta = \frac{\alpha}{\sigma_1} \quad (3)$$

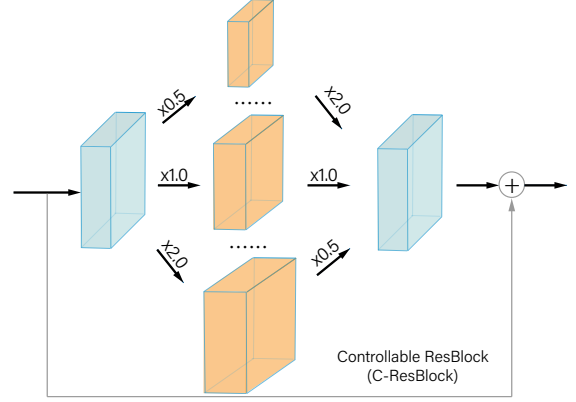


Figure 4. Overview of the proposed Controllable Residual Block (C-ResBlock). Based on the bottleneck ratio (e.g., 0.5, 1.0, 2.0), C-ResBlock contains fully connected layers either in a squeeze-expand or expand-squeeze manner. This allow us to conveniently balance between model size and model performance.

Based on the analysis above, we consider three scenarios, where we adopt different strategies for normalization (Fig. 3). (1) If  $\sigma_1 < \alpha$ , the grouped points are too close to the sampled points (i.e., the point cloud is dense). In this case, we have  $\Delta > 1$ , meaning we are pulling the grouped points apart, which raises the standard deviation and reduces the density of the point cloud. (2) If  $\sigma_1 > \alpha$ , the grouped points are too far away from the sampled points (i.e., the point cloud is sparse). In this case, we have  $\Delta < 1$ , meaning we are pushing the grouped points together, which reduces the standard deviation and increases the density of the point cloud. (3) If  $\sigma_1 = \alpha$ , we have  $\Delta = 1$ . In this case, there is no need to push or pull the grouped point, and the standard deviation stays the same. Since  $\alpha$  is learnable, our normalization operations can optimize such ‘push-and-pull’ strategy during model training so that we can adaptively adjust the point cloud density in the goal of better accuracy. In this way, we effectively and efficiently address the irregularity of point cloud.

### 3.2. Controllable Residual Block

The Residual Block (ResBlock) [9] is initially designed for 2D image classification tasks. Recently, PointMLP [23] has adapted ResBlock for MLP-based point cloud analysis by changing all convolution layers to fully connected layers. Aiming to design a lightweight model, we revisit two popular variants of ResBlock. The first variant is the Inverted Residual Block (InvResBlock) [35], which can promote computational efficiency but have many parameters. The second variant is the squeeze-and-excitation block (SE-Block) [10], which can reduce the number of parameters but rely on the average pooling operation, which is ineffective

for the MLP-based model [18]. In this work, we seek to combine the advantage of InvResBlock and SEBlock and design a new Controllable Residual Block (C-ResBlock). C-ResBlock eliminates the need for pooling layers and only needs an arbitrary bottleneck ratio for channel number reduction and channel number promotion. Despite its simplicity, C-ResBlock still delivers excellent computational efficiency, small numbers of parameters, and good classification accuracy, according to our experiments and ablation studies. The workflow for C-ResBlock is shown in Fig. 4.

### 3.3. PointNorm

We show the workflow of PointNorm in Fig. 2. PointNorm can be divided into five steps: feature embedding, sampling-grouping, DualNorm (Point Normalization + Reverse Point Normalization), non-linear mapping, and classification. The feature embedding step aims to raise the channel number so the network contains more learnable parameters. Inspired by PointNet++ [32], the sampling-grouping, the DualNorm, and the non-linear mapping step are repeated three times to extract hierarchical features with different receptive fields progressively. We use Farthest Point Sampling (FPS) [25, 32, 41, 23] for point sampling, and we use K-Nearest Neighbors (KNN) with  $k = 24$  [29, 17, 41, 43, 23] for point grouping. Following sampling-grouping, we leverage DualNorm to normalize the sampled and the grouped points. Following DualNorm, the sampled and the grouped points are concatenated before entering the subsequent non-linear mapping step. The non-linear mapping step consists of four Controllable Residual Blocks and one max pooling layer in the middle for channel number reduction. Finally, inspired by previous works [31, 32, 57, 43], we use a max pooling layer before the classifier to preserve only the salient features for the classification step. The supplementary material will include PointNorm’s architecture for part segmentation tasks.

### 3.4. PointNorm-Tiny

Although PointNorm has excellent inference latency and classification accuracy, it has a relatively large amount of parameters (12.63M). This motivates us to design a lightweight version essential for mobile deployment. Ideally, the lightweight version should have a small amount of parameters, a substantial inference latency, and a promising classification accuracy. To this end, we make three modifications to PointNorm to obtain the lightweight version called PointNorm-Tiny. Firstly, we decrease the bottleneck ratio for each C-ResBlock from 1.00 to 0.25. Secondly, we reduce the embedding dimension for the feature embedding step from 64 to 32. Finally, we reduce the C-ResBlock number by 50%. The proposed PointNorm-Tiny has only 0.68M parameters; it inferences faster than PointNet++; and it delivers excellent classification accuracy in the experiments.

## 4. Experiments

In this section, we first describe the implementation details of PointNorm and then compare PointNorm with state-of-the-art methods on shape classification and part segmentation benchmarks. Finally, we conduct ablation studies to demonstrate the effectiveness of the proposed modules and the reason for the current hyperparameter selection.

### 4.1. Implementation Details

For the experiments on ScanObjectNN dataset, PointNorm is trained on a single GPU for 200 epochs, using Pytorch [27] as the framework and AdamW [22] as the optimizer. The initial learning rate is 0.01, and a cosine annealing scheduler [21] gradually reduces the learning rate to 0.0001. The batch size is 32; the embedding dimension is 64; and it takes approximately 9 hours to converge the model.

Based on the results from Subsection 4.4, we utilize both point normalization and reverse point normalization, adopt local mean and global standard deviation, and choose C-ResBlock with a bottleneck ratio of 1.0. Inspired by previous works [43, 23], we use cross-entropy with label smoothing [38] as the loss function. Finally, we adopt the widely used [32, 43, 39, 23] random rotation and translation [32] as the data augmentation techniques. The implementation details on ModelNet40 and ShapeNetPart datasets will be in the supplementary material.

### 4.2. Shape Classification

We evaluate PointNorm on shape classification tasks, using two benchmark datasets. The first benchmark is ModelNet40 [45] dataset, a synthetic dataset with 40 classes, 9,843 training samples, and 581 testing samples. The second benchmark is ScanobjectNN [40] dataset, a real-world dataset with 15 classes, 2,321 training samples, and 581 testing samples.

We show the experiment results for shape classification in Table 1<sup>2</sup>. On ScanObjectNN dataset, PointNorm has the best OA of 86.8% and the best mAcc of 85.6%. Notably, PointNorm surpasses the recent state-of-the-art PointMLP by 1.4% for OA and 1.7% for mAcc. On ModelNet40 dataset, PointNorm has the best mAcc of 91.3% and the second-best OA of 93.7%, only 0.1% less than the recent state-of-the-art CurveNet (93.8%). However, we note that the train speed of PointNorm (58.2 samples/second) is approximately 2 times faster than CurveNet (20.8 samples/second), and the test speed of PointNorm (140.0 sam-

<sup>2</sup>PointMLP’s result on ModelNet40 dataset are taken from PointMLP’s official code repository: <https://github.com/ma-xu/pointMLP-pytorch/issues/1>. RepSurf reports accuracy on both ModelNet40 and ScanObjectNN. However, its code and pretrained model for ModelNet40 are missing. Therefore, we remove RepSurf’s result on ModelNet40 from the table and indicate it is unavailable.

Method	Publication	Input	ModelNet40 [45]		ScanObjectNN [40]		#Params	Train Speed	Test Speed
			OA (%)	mAcc (%)	OA (%)	mAcc (%)			
PointNet [31]	CVPR 2017	1k	89.2	86.0	68.2	63.4	3.47M	-	-
PointNet++ [32]	NeurIPS 2017	1k	90.7	88.4	77.9	75.4	1.48M	<b>223.8</b>	<b>308.5</b>
PointCNN [17]	NeurIPS 2018	1k	92.5	88.1	78.5	75.1	-	-	-
DGCNN [43]	TOG 2019	1k	92.9	90.2	78.1	73.6	1.82M	-	-
RS-CNN [20]	CVPR 2019	1k	92.9	-	-	-	2.38M	-	-
PointConv [44]	CVPR 2019	1k	92.5	-	-	-	18.6M	17.9	10.2
KPConv [39]	ICCV 2019	7k	92.9	-	-	-	14.3M	31.0	80.0
PointASNL [51]	CVPR 2020	1k	93.2	-	-	-	10.1M	-	-
Grid-GCN [49]	CVPR 2020	1k	93.1	<b>91.3</b>	-	-	-	-	-
DRNet [33]	WACV 2021	1k	93.1	-	80.3	78.0	-	-	-
PAConv [47]	CVPR 2021	1k	93.6	-	-	-	2.44M	-	-
CurveNet [46]	ICCV 2021	1k	<b>93.8</b>	-	-	-	2.04M	20.8	15.0
GDANet [48]	AAAI 2021	1k	93.4	-	-	-	<b>0.93M</b>	26.3	14.0
PRANet [5]	TIP 2021	1k	93.2	90.6	81.0	77.9	-	-	-
PointMLP [23]	ICLR 2022	1k	<b>93.7</b>	<b>90.9</b>	<b>85.4</b>	<b>83.9</b>	12.60M	47.1	112.0
RepSurf-U [34]	CVPR 2022	1k	-	-	84.6	81.9	1.48M	-	-
PointNorm		1k	<b>93.7</b>	<b>91.3</b>	<b>86.8</b>	<b>85.6</b>	12.63M	58.2	140.0
PointNorm-Tiny		1k	93.5	90.6	85.3	83.6	<b>0.68M</b>	<b>196.4</b>	<b>420.0</b>

Table 1. Shape Classification Result on ModelNet40 and ScanObjectNN dataset. All methods except PointASNL are tested **without the voting strategy**. We use overall accuracy (OA) and mean accuracy (mAcc), number of parameters (#Params), train speed and test speed by samples per second computed on a single GPU as the evaluation metrics. We use **bold** to indicate the best score, and **blue** for the second-best score. '-' indicate a result is unavailable.

Method	Inst. mIoU	Cls. mIoU	air-plane	bag	cap	car	chair	aero-phone	guitar	knife	lamp	laptop	motor-bike	mug	pistol	rocket	skate-board	table
PointNet [31]	83.7	80.4	83.4	78.7	82.5	74.9	89.6	73.0	91.5	85.9	80.8	95.3	65.2	93.0	81.2	57.9	72.8	80.6
PointNet++ [32]	85.1	81.9	82.4	79.0	87.7	77.3	90.8	71.8	91.0	85.9	83.7	95.3	71.6	94.1	81.3	58.7	76.4	82.6
PCNN [2]	85.1	81.8	82.4	80.1	85.5	79.5	90.8	73.2	91.3	86.0	85.0	95.7	73.2	94.8	83.3	51.0	75.0	81.8
DGCNN [43]	85.2	82.3	84.0	83.4	86.7	77.8	90.6	74.7	91.2	87.5	82.8	95.7	66.3	94.9	81.1	63.5	74.5	82.6
PointCNN [17]	86.1	84.6	84.1	86.5	86.0	80.8	90.6	79.7	92.3	88.4	85.3	96.1	77.2	95.2	84.2	64.2	80.0	83.0
RS-CNN [20]	<b>86.2</b>	84.0	83.5	84.8	88.8	79.6	91.2	81.1	91.6	88.4	86.0	96.0	73.7	94.1	83.4	60.5	77.7	83.6
SyncSpecCNN [54]	84.7	82.0	81.6	81.7	81.9	75.2	90.2	74.9	93.0	86.1	84.7	95.6	66.7	92.7	81.6	60.6	82.9	82.1
SPLATNet [37]	85.4	83.7	83.2	84.3	89.1	80.3	90.7	75.5	92.1	87.1	83.9	96.3	75.6	95.8	83.8	64.0	75.5	81.8
SpiderCNN [50]	85.3	82.4	83.5	81.0	87.2	77.5	90.7	76.8	91.1	87.3	83.3	95.8	70.2	93.5	82.7	59.7	75.8	82.8
PAConv [47]	86.1	84.6	84.3	85.0	90.4	79.7	90.6	80.8	92.0	88.7	82.2	95.9	73.9	94.7	84.7	65.9	81.4	84.0
PointMLP [23]	86.1	84.6	83.5	83.4	87.5	80.5	90.3	78.2	92.2	88.1	82.6	96.2	77.5	95.8	85.4	64.6	83.3	84.3
PointNorm	<b>86.2</b>	<b>84.7</b>	82.7	84.9	88.9	79.8	90.2	81.9	91.6	87.4	82.9	95.8	78.4	95.5	84.5	65.6	81.4	83.8
PointNorm-Tiny	85.6	84.5	82.9	88.0	89.7	79.3	90.1	79.9	91.6	87.7	82.4	95.8	76.3	95.0	83.5	64.6	81.9	83.5

Table 2. Part Segmentation Result on ShapeNetPart dataset. The best score for Instance mIoU and Class mIoU are in **bold**. Zoom in to view better.

ples/second) is more than 8 times faster than CurveNet (15.0 samples/second). In point cloud analysis, where computational efficiency is of significant priority [7], The clear advantage in train and test speed should be more critical than the 0.1% gap for OA.

As mentioned in Subsection 3.4, the introduction of PointNorm-Tiny aims to enhance the training and testing speed and, more importantly, reduce the number of parameters. It is worth mentioning that PointNorm-Tiny has the smallest number of parameters (0.68M), the best test speed (420.0 samples/second), and the second-best train speed (196.4 samples/second). Although it is lightweight and computationally efficient, PointNorm-Tiny delivers promising results on ModelNet40 and ScanObjectNN, surpassing recent state-of-the-art methods like PRANet [5] and DRNet [33].

### 4.3. Part Segmentation

We evaluate our PointNorm on the part segmentation task, using ShapeNetPart [53] as the benchmark dataset. The ShapeNetPart dataset contains 16,881 shapes, 16 classes, and 50 parts labels. The experiment results for part segmentation are in Table 2. We can see that PointNorm achieves the best score for both instance mIoU (86.2%) and class mIoU (84.7%). Our PointNorm-Tiny is the smallest model in the table. However, it still delivers compelling (85.6%) instance mIoU and class mIoU (84.5%). Notably, PointNorm-Tiny’s class IoU for the bag is 88.0%, which is the best among all methods. We also visualize the part segmentation results in Fig. 7. It can be seen that both PointNorm and PointNorm-Tiny’s predictions are incredibly close to the ground truth. More part segmentation results will be in the supplementary material.



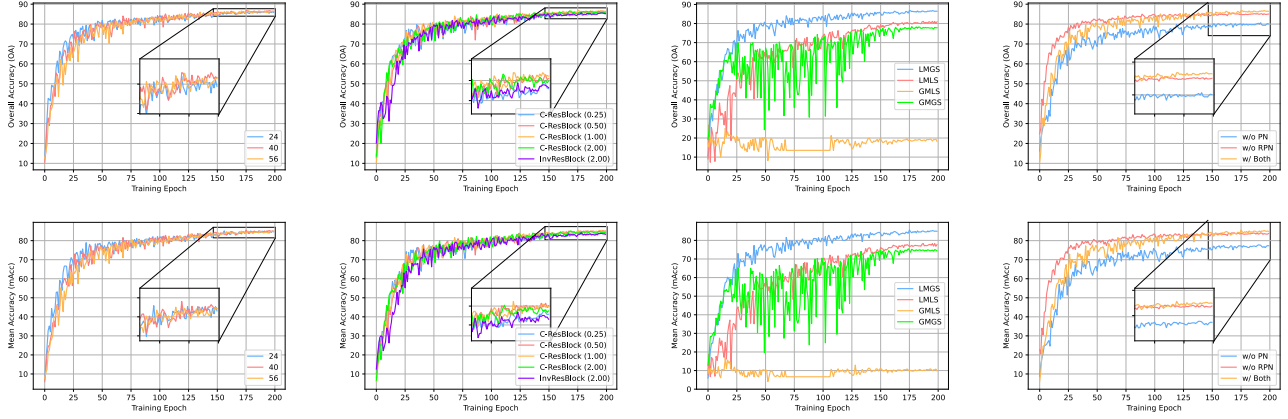


Figure 5. Testing Accuracy Curve for different variants of PointNorm. Top/Bottom Row: Overall Accuracy (OA)/Mean Accuracy (mAcc) to Training Epochs. Both OA and mAcc are reported in %. Zoom in for better view.

		OA(%)	mAcc(%)	FLOPs	#Params	Train Time	Test Time
Layer Number	24	86.5	85.2	8.71G	7.30M	99	9
	40	<b>86.8</b>	<b>85.6</b>	14.59G	12.63M	145	13
	56	86.7	85.0	20.48G	17.95M	190	16
Block (Ratio)	C-ResBlock (0.25)	85.9	84.5	5.79G	4.65M	99	9
	C-ResBlock (0.5)	86.6	85.4	8.72G	7.31M	111	10
	C-ResBlock (1.0)	<b>86.8</b>	<b>85.6</b>	14.59G	12.63M	145	13
	C-ResBlock (2.0)	86.6	85.1	26.34G	23.27M	205	17
	InvResBlock (2.0)	85.8	84.2	26.46G	23.34M	252	21
Local/Global	LMGS	<b>86.8</b>	<b>85.6</b>	14.59G	12.63M	145	13
	LMLS	81.2	78.3	14.59G	12.63M	145	13
	GMLS	25.1	16.8	14.59G	12.63M	143	13
	GMGS	78.4	75.5	14.59G	12.63M	143	13
Normalization	w/o PN	80.7	77.8	14.59G	12.63M	136	12
	w/o RPN	85.6	84.1	14.59G	12.63M	141	12
	w/ both	<b>86.8</b>	<b>85.6</b>	14.59G	12.63M	145	13

Table 3. Ablation Result for PointNorm’s shape classification on ScanObjectNN Dataset. FLOPs refers to the floating-point operations for computing a point cloud consisting of 1024 points. Train/Test Time refers to the seconds per epoch on the training/testing dataset. We use **bold** to indicate the best score.

#### 4.4. Ablation Studies

We conduct extensive ablation studies on ScanObjectNN dataset to demonstrate the effectiveness of the proposed component in PointNorm, and the reason for specific module designs and hyperparameters selections. We employ score table (Table 3), accuracy curve (Fig. 5), and loss landscape (Fig. 6) to investigate four aspects, including Layer Number, Bottleneck Ratio, Local and Global Choice, and Component Studies.

**Layer Number** We define the Layer Number as the number of learnable layers in a network except for batch normalization and activation functions. Indeed, we can easily adjust the Layer Number by changing the numbers of C-Resblock in PointNorm. Table 3 shows that the 40-layer variant gives the best OA and mAcc. Besides, the first col-

umn of Fig. 5 displays that the 40-layer variant has the most consistent accuracy growth and the most stable model convergence. However, all Layer Number variants of PointNorm (24-layer, 40-layer, 56-layer) have a close OA and mAcc, much better than the previous state-of-the-art. That demonstrates the robustness of PointNorm to Layer Number in the network.

**Bottleneck Ratio** The Bottleneck Ratio aims to effectively trade-off between model size and model performance. We consider four bottleneck ratios (0.25, 0.50, 1.00, 2.00) to analyze our C-ResBlock’s performance at different scales. We additionally add InvResBlock with a bottleneck ratio of 2.0 to aid comparison. From Table 3, we find that C-ResBlock (1.0) gives the best OA and mAcc. However, we can sacrifice 0.2% OA and mAcc to build a lightweight version C-

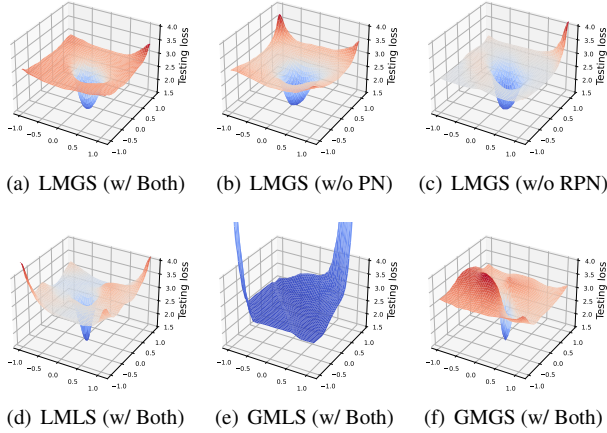


Figure 6. Loss landscape [16] along two random directions for different variants of PointNorm. Zoom in to view the details. The loss landscape visualization for other PointNorm variants will be in the supplementary material.

ResBlock (0.5), which has better computational efficiency and a smaller model size.

Besides, we find that C-ResBlock performs better than InvResBlock, under the same or even with smaller bottleneck ratios. For example, C-ResBlock (2.0) surpasses InvResBlock (2.0) by 0.8% in OA and 0.9% in mAcc, while still having better FLOPs, Params, Train Time, and Test Time. C-ResBlock’s superiority is more evident in the second column of Fig. 5. With approximately 22% FLOPs and 20% Params, C-ResBlock (0.25) outperforms InvResBlock (2.0) for both OA and mAcc towards the end of training. Based on the analysis above, we conclude that C-ResBlock with a bottleneck ratio of 1.0 is the optimal choice, and C-ResBlock is better than the widely used InvResBlock under all given bottleneck ratios.

**Local and Global Choice** As mentioned in Subsection 3.1, we can choose either *Local* or *Global* for calculating the mean and the standard deviation. Therefore, there exists four combinations, including Local Mean Global Standard Deviation (LMGS), Local Mean Local Standard Deviation (LMLS), Global Mean Local Standard Deviation (GMLS), and Global Mean Global Standard Deviation (GMGS).

Table 3 and the third column of Fig. 5 show that GMLS’s OA and mAcc stuck at a low score and that GMGS’s OA and mAcc have significant fluctuations. In comparison, LMLS and LMGS have more consistent growth patterns for OA and mAcc. However, LMGS has remarkably better scores for both OA and mAcc. The loss landscape visualization in Fig. 6 shows that LMLS and GMGS have very sharp minimas and rough landscapes with many hills, which is hard to train. GMLS cannot be optimized because it has no apparent minima. In comparison, LMGS has a flat minima and a smooth landscape, which remarkably facili-

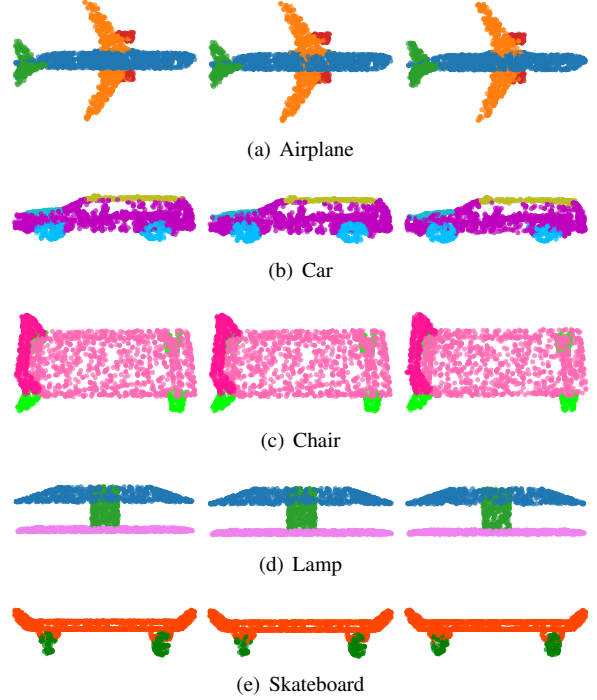


Figure 7. Part Segmentation Result Visualization. From left to right column: Ground Truth, PointNorm, PointNorm-Tiny. Best viewed in color.

ties the optimization process [13, 16]. Based upon the analysis above, we conclude that Local Mean Global Standard Deviation (LMGS) is the optimal choice.

**Component Studies** We conduct ablation studies on the two components of the DualNorm module: Point Normalization (PN) and Reverse Point Normalization (RPN). We consider three variants, including PointNorm without (w/o) PN, PointNorm without (w/o) RPN, and PointNorm with (w/) both PN and RPN.

Table 3 and the fourth column of Fig. 5 show that PointNorm w/ Both PN and RPN has the best OA and mAcc. In comparison, PointNorm w/o PN has a significantly lower OA and mAcc. PointNorm w/o RPN has better OA and mAcc in the starting 125 epochs but lower OA and mAcc at the final 75 epochs than PointNorm w/ Both PN and RPN. The loss landscape visualization in Fig. 6 show that PointNorm w/ Both PN and RPN has a flat minima and a smooth landscape. Although PointNorm w/o PN and PointNorm w/o RPN also have a flat minima, they have significant up-hills at the border which may drive the loss up. Besides, their landscapes are less smooth. Based on the analysis above, we conclude that both PN and RPN are essential.

## 5. Conclusion

In this paper, we proposed PointNorm, a simple MLP-based point cloud analysis network that eliminates the need



for sophisticated feature extractors. The key ingredient of PointNorm is the DualNorm module, where we normalize the grouped points and the sampled points to each other using local mean and global standard deviation. With this straightforward design, we leveraged both local and global features to improve the classification accuracy while enjoying a faithful inference latency. Comprehensive experiments and ablation studies have demonstrated the effectiveness of the proposed method.

We sincerely hope this work will inspire the point cloud analysis community to slow down the competition for sophisticated feature extractors and complex model architectures and to revisit the succinct design philosophy. In the future, we plan to embed the DualNorm module into other architectures like PointNet++ [32]. We also hope to apply PointNorm to object detection (e.g., SUN RGB-D [36]) and semantic segmentation (e.g., S3DIS [1]) tasks.

## References

- [1] Iro Armeni, Ozan Sener, Amir R Zamir, Helen Jiang, Ioannis Brilakis, Martin Fischer, and Silvio Savarese. 3d semantic parsing of large-scale indoor spaces. In *Proceedings of the IEEE conference on computer vision and pattern recognition*, pages 1534–1543, 2016.
- [2] Matan Atzmon, Haggai Maron, and Yaron Lipman. Point convolutional neural networks by extension operators. *arXiv preprint arXiv:1803.10091*, 2018.
- [3] Saifullahi Aminu Bello, Shangshu Yu, Cheng Wang, Jibril Muhmmad Adam, and Jonathan Li. Deep learning on 3d point clouds. *Remote Sensing*, 12(11):1729, 2020.
- [4] Siheng Chen, Baoan Liu, Chen Feng, Carlos Vallespi-Gonzalez, and Carl Wellington. 3d point cloud processing and learning for autonomous driving: Impacting map creation, localization, and perception. *IEEE Signal Processing Magazine*, 38(1):68–86, 2020.
- [5] Silin Cheng, Xiwu Chen, Xinwei He, Zhe Liu, and Xiang Bai. Pra-net: Point relation-aware network for 3d point cloud analysis. *IEEE Transactions on Image Processing*, 30:4436–4448, 2021.
- [6] Meng-Hao Guo, Jun-Xiong Cai, Zheng-Ning Liu, Tai-Jiang Mu, Ralph R Martin, and Shi-Min Hu. Pct: Point cloud transformer. *Computational Visual Media*, 7(2):187–199, 2021.
- [7] Yulan Guo, Hanyun Wang, Qingyong Hu, Hao Liu, Li Liu, and Mohammed Bennamoun. Deep learning for 3d point clouds: A survey. *IEEE transactions on pattern analysis and machine intelligence*, 43(12):4338–4364, 2020.
- [8] Abdullah Hamdi, Silvio Giancola, and Bernard Ghanem. Mvtn: Multi-view transformation network for 3d shape recognition. In *Proceedings of the IEEE/CVF International Conference on Computer Vision*, pages 1–11, 2021.
- [9] Kaiming He, Xiangyu Zhang, Shaoqing Ren, and Jian Sun. Deep residual learning for image recognition. In *Proceedings of the IEEE conference on computer vision and pattern recognition*, pages 770–778, 2016.
- [10] Jie Hu, Li Shen, and Gang Sun. Squeeze-and-excitation networks. In *Proceedings of the IEEE conference on computer vision and pattern recognition*, pages 7132–7141, 2018.
- [11] Lei Huang, Jie Qin, Yi Zhou, Fan Zhu, Li Liu, and Ling Shao. Normalization techniques in training dnns: Methodology, analysis and application. *arXiv preprint arXiv:2009.12836*, 2020.
- [12] Sergey Ioffe and Christian Szegedy. Batch normalization: Accelerating deep network training by reducing internal covariate shift. In *International conference on machine learning*, pages 448–456. PMLR, 2015.
- [13] Nitish Shirish Keskar, Dheevatsa Mudigere, Jorge Nocedal, Mikhail Smelyanskiy, and Ping Tak Peter Tang. On large-batch training for deep learning: Generalization gap and sharp minima. *arXiv preprint arXiv:1609.04836*, 2016.
- [14] Alon Lahav and Ayellet Tal. Meshwalker: Deep mesh understanding by random walks. *ACM Transactions on Graphics (TOG)*, 39(6):1–13, 2020.
- [15] Loic Landrieu and Martin Simonovsky. Large-scale point cloud semantic segmentation with superpoint graphs. In *Proceedings of the IEEE conference on computer vision and pattern recognition*, pages 4558–4567, 2018.
- [16] Hao Li, Zheng Xu, Gavin Taylor, Christoph Studer, and Tom Goldstein. Visualizing the loss landscape of neural nets. *Advances in neural information processing systems*, 31, 2018.
- [17] Yangyan Li, Rui Bu, Mingchao Sun, Wei Wu, Xinhan Di, and Baoquan Chen. Pointcnn: Convolution on x-transformed points. *Advances in neural information processing systems*, 31, 2018.
- [18] Min Lin, Qiang Chen, and Shuicheng Yan. Network in network. *arXiv preprint arXiv:1312.4400*, 2013.
- [19] Zhi-Hao Lin, Sheng-Yu Huang, and Yu-Chiang Frank Wang. Convolution in the cloud: Learning deformable kernels in 3d graph convolution networks for point cloud analysis. In *Proceedings of the IEEE/CVF conference on computer vision and pattern recognition*, pages 1800–1809, 2020.
- [20] Yongcheng Liu, Bin Fan, Shiming Xiang, and Chunhong Pan. Relation-shape convolutional neural network for point cloud analysis. In *Proceedings of the IEEE/CVF Conference on Computer Vision and Pattern Recognition*, pages 8895–8904, 2019.
- [21] Ilya Loshchilov and Frank Hutter. Sgdr: Stochastic gradient descent with warm restarts. *arXiv preprint arXiv:1608.03983*, 2016.
- [22] Ilya Loshchilov and Frank Hutter. Decoupled weight decay regularization. *arXiv preprint arXiv:1711.05101*, 2017.
- [23] Xu Ma, Can Qin, Haoxuan You, Haoxi Ran, and Yun Fu. Rethinking network design and local geometry in point cloud: A simple residual mlp framework. *arXiv preprint arXiv:2202.07123*, 2022.
- [24] Daniel Maturana and Sebastian Scherer. Voxnet: A 3d convolutional neural network for real-time object recognition. In *2015 IEEE/RSJ international conference on intelligent robots and systems (IROS)*, pages 922–928. IEEE, 2015.
- [25] Carsten Moenning and Neil A Dodgson. Fast marching farthest point sampling. Technical report, University of Cambridge, Computer Laboratory, 2003.

- [26] Dejing Ni, Andrew YC Nee, Soh-Khim Ong, Huijun Li, Chengcheng Zhu, and Aiguo Song. Point cloud augmented virtual reality environment with haptic constraints for teleoperation. *Transactions of the Institute of Measurement and Control*, 40(15):4091–4104, 2018.
- [27] Adam Paszke, Sam Gross, Francisco Massa, Adam Lerer, James Bradbury, Gregory Chanan, Trevor Killeen, Zeming Lin, Natalia Gimelshein, Luca Antiga, et al. Pytorch: An imperative style, high-performance deep learning library. *Advances in neural information processing systems*, 32, 2019.
- [28] S Patro and Kishore Kumar Sahu. Normalization: A preprocessing stage. *arXiv preprint arXiv:1503.06462*, 2015.
- [29] Leif E Peterson. K-nearest neighbor. *Scholarpedia*, 4(2):1883, 2009.
- [30] François Pomerleau, Francis Colas, Roland Siegwart, et al. A review of point cloud registration algorithms for mobile robotics. *Foundations and Trends® in Robotics*, 4(1):1–104, 2015.
- [31] Charles R Qi, Hao Su, Kaichun Mo, and Leonidas J Guibas. Pointnet: Deep learning on point sets for 3d classification and segmentation. In *Proceedings of the IEEE conference on computer vision and pattern recognition*, pages 652–660, 2017.
- [32] Charles Ruizhongtai Qi, Li Yi, Hao Su, and Leonidas J Guibas. Pointnet++: Deep hierarchical feature learning on point sets in a metric space. *Advances in neural information processing systems*, 30, 2017.
- [33] Shi Qiu, Saeed Anwar, and Nick Barnes. Dense-resolution network for point cloud classification and segmentation. In *Proceedings of the IEEE/CVF Winter Conference on Applications of Computer Vision*, pages 3813–3822, 2021.
- [34] Haoxi Ran, Jun Liu, and Chengjie Wang. Surface representation for point clouds. In *Proceedings of the IEEE/CVF Conference on Computer Vision and Pattern Recognition*, pages 18942–18952, 2022.
- [35] Mark Sandler, Andrew Howard, Menglong Zhu, Andrey Zhmoginov, and Liang-Chieh Chen. Mobilenetv2: Inverted residuals and linear bottlenecks. In *Proceedings of the IEEE conference on computer vision and pattern recognition*, pages 4510–4520, 2018.
- [36] Shuran Song, Samuel P Lichtenberg, and Jianxiong Xiao. Sun rgb-d: A rgb-d scene understanding benchmark suite. In *Proceedings of the IEEE conference on computer vision and pattern recognition*, pages 567–576, 2015.
- [37] Hang Su, Varun Jampani, Deqing Sun, Subhransu Maji, Evangelos Kalogerakis, Ming-Hsuan Yang, and Jan Kautz. Splatnet: Sparse lattice networks for point cloud processing. In *Proceedings of the IEEE conference on computer vision and pattern recognition*, pages 2530–2539, 2018.
- [38] Christian Szegedy, Vincent Vanhoucke, Sergey Ioffe, Jon Shlens, and Zbigniew Wojna. Rethinking the inception architecture for computer vision. In *Proceedings of the IEEE conference on computer vision and pattern recognition*, pages 2818–2826, 2016.
- [39] Hugues Thomas, Charles R Qi, Jean-Emmanuel Deschaud, Beatriz Marcotequi, François Goulette, and Leonidas J Guibas. Kpconv: Flexible and deformable convolution for point clouds. In *Proceedings of the IEEE/CVF international conference on computer vision*, pages 6411–6420, 2019.
- [40] Mikaela Angelina Uy, Quang-Hieu Pham, Binh-Son Hua, Thanh Nguyen, and Sai-Kit Yeung. Revisiting point cloud classification: A new benchmark dataset and classification model on real-world data. In *Proceedings of the IEEE/CVF international conference on computer vision*, pages 1588–1597, 2019.
- [41] Chu Wang, Babak Samari, and Kaleem Siddiqi. Local spectral graph convolution for point set feature learning. In *Proceedings of the European conference on computer vision (ECCV)*, pages 52–66, 2018.
- [42] Xiaolong Wang, Ross Girshick, Abhinav Gupta, and Kaiming He. Non-local neural networks. In *Proceedings of the IEEE conference on computer vision and pattern recognition*, pages 7794–7803, 2018.
- [43] Yue Wang, Yongbin Sun, Ziwei Liu, Sanjay E Sarma, Michael M Bronstein, and Justin M Solomon. Dynamic graph cnn for learning on point clouds. *Acm Transactions On Graphics (tog)*, 38(5):1–12, 2019.
- [44] Wenxuan Wu, Zhongang Qi, and Li Fuxin. Pointconv: Deep convolutional networks on 3d point clouds. In *Proceedings of the IEEE/CVF Conference on Computer Vision and Pattern Recognition*, pages 9621–9630, 2019.
- [45] Zhirong Wu, Shuran Song, Aditya Khosla, Fisher Yu, Linguang Zhang, Xiaoou Tang, and Jianxiong Xiao. 3d shapenets: A deep representation for volumetric shapes. In *Proceedings of the IEEE conference on computer vision and pattern recognition*, pages 1912–1920, 2015.
- [46] Tiange Xiang, Chaoyi Zhang, Yang Song, Jianhui Yu, and Weidong Cai. Walk in the cloud: Learning curves for point clouds shape analysis. In *Proceedings of the IEEE/CVF International Conference on Computer Vision*, pages 915–924, 2021.
- [47] Mutian Xu, Runyu Ding, Hengshuang Zhao, and Xiaojuan Qi. Paconv: Position adaptive convolution with dynamic kernel assembling on point clouds. In *Proceedings of the IEEE/CVF Conference on Computer Vision and Pattern Recognition*, pages 3173–3182, 2021.
- [48] Mutian Xu, Junhao Zhang, Zhipeng Zhou, Mingye Xu, Xiaojuan Qi, and Yu Qiao. Learning geometry-disentangled representation for complementary understanding of 3d object point cloud. In *Proceedings of the AAAI Conference on Artificial Intelligence*, volume 35, pages 3056–3064, 2021.
- [49] Qiangeng Xu, Xudong Sun, Cho-Ying Wu, Panqu Wang, and Ulrich Neumann. Grid-gcn for fast and scalable point cloud learning. In *Proceedings of the IEEE/CVF Conference on Computer Vision and Pattern Recognition*, pages 5661–5670, 2020.
- [50] Yifan Xu, Tianqi Fan, Mingye Xu, Long Zeng, and Yu Qiao. Spidercnn: Deep learning on point sets with parameterized convolutional filters. In *Proceedings of the European Conference on Computer Vision (ECCV)*, pages 87–102, 2018.
- [51] Xu Yan, Chaoda Zheng, Zhen Li, Sheng Wang, and Shuguang Cui. Pointasnl: Robust point clouds processing using nonlocal neural networks with adaptive sampling. In *Proceedings of the IEEE/CVF Conference on Computer Vision and Pattern Recognition*, pages 5589–5598, 2020.

- [52] Zetong Yang, Yanan Sun, Shu Liu, Xiaoyong Shen, and Jiaya Jia. Std: Sparse-to-dense 3d object detector for point cloud. In *Proceedings of the IEEE/CVF international conference on computer vision*, pages 1951–1960, 2019.
- [53] Li Yi, Vladimir G Kim, Duygu Ceylan, I-Chao Shen, Mengyan Yan, Hao Su, Cewu Lu, Qixing Huang, Alla Sheffer, and Leonidas Guibas. A scalable active framework for region annotation in 3d shape collections. *ACM Transactions on Graphics (ToG)*, 35(6):1–12, 2016.
- [54] Li Yi, Hao Su, Xingwen Guo, and Leonidas J Guibas. Sync-specnn: Synchronized spectral cnn for 3d shape segmentation. In *Proceedings of the IEEE conference on computer vision and pattern recognition*, pages 2282–2290, 2017.
- [55] Haoxuan You, Yifan Feng, Rongrong Ji, and Yue Gao. Pvnnet: A joint convolutional network of point cloud and multi-view for 3d shape recognition. In *Proceedings of the 26th ACM international conference on Multimedia*, pages 1310–1318, 2018.
- [56] Hengshuang Zhao, Li Jiang, Jiaya Jia, Philip HS Torr, and Vladlen Koltun. Point transformer. In *Proceedings of the IEEE/CVF International Conference on Computer Vision*, pages 16259–16268, 2021.
- [57] Yin Zhou and Oncel Tuzel. Voxelnet: End-to-end learning for point cloud based 3d object detection. In *Proceedings of the IEEE conference on computer vision and pattern recognition*, pages 4490–4499, 2018.